coatings

MDPI

Article

Low-Temperature CVD-Grown Graphene Thin Films as Transparent Electrode for Organic Photovoltaics

Alaa Y. Ali [1,2], Natalie P. Holmes [1,3], Mohsen Ameri [4], Krishna Feron [1], Mahir N. Thameel [5], Matthew G. Barr [1], Adam Fahy [1], John Holdsworth [1], Warwick Belcher [1], Paul Dastoor [1,*] and Xiaojing Zhou [1,*]

1 Center of Organic Electronics, University of Newcastle, Newcastle 2308, Australia; alaa.y.ali@tu.edu.iq (A.Y.A.); natalie.holmes@sydney.edu.au (N.P.H.); krishna.feron@newcastle.edu.au (K.F.); matthew.barr@newcastle.edu.au (M.G.B.); adam.fahy@newcastle.edu.au (A.F.); john.holdsworth@newcastle.edu.au (J.H.); warwick.belcher@newcastle.edu.au (W.B.)
2 Department of Physics, College of Education for Pure Science, University of Tikrit, Tikrit 34001, Iraq
3 Australian Centre for Microscopy and Microanalysis, University of Sydney, Sydney 2006, Australia
4 Electrical & Computer Engineering, University of Alabama, Tuscaloosa, AL 35487, USA; mameri@ua.edu
5 Department of Physics, College of Education for Pure Science, University of Anbar, Ramadi 31001, Iraq; eps.mahern.thumail@uonanbar.edu.iq
* Correspondence: paul.dastoor@newcastle.edu.au (P.D.); xiaojing.zhou@newcastle.edu.au (X.Z.)

Abstract: Good conductivity, suitable transparency and uniform layers of graphene thin film can be produced by chemical vapour deposition (CVD) at low temperature and utilised as a transparent electrode in organic photovoltaics. Using chlorobenzene trapped in poly(methyl methacrylate) (PMMA) polymer as the carbon source, growth temperature (T_{growth}) of 600 °C at hydrogen (H_2) flow of 75 standard cubic centimetres per minute (sccm) was used to prepare graphene by CVD catalytically on copper (Cu) foil substrates. Through the T_{growth} of 600 °C, we observed and identified the quality of the graphene films, as characterised by Raman spectroscopy. Finally, P3HT (poly (3-hexylthiophene-2, 5-diyl)): PCBM (phenyl-C_{61}-butyric acid methyl ester) bulk heterojunction solar cells were fabricated on graphene-based window electrodes and compared with indium tin oxide (ITO)-based devices. It is interesting to observe that the OPV performance is improved more than 5 fold with increasing illuminated areas, hinting that high resistance between graphene domains can be alleviated by photo generated charges.

Keywords: graphene thin film; low-temperature CVD; organic photovoltaics

check for updates

Citation: Ali, A.Y.; Holmes, N.P.; Ameri, M.; Feron, K.; Thameel, M.N.; Barr, M.G.; Fahy, A.; Holdsworth, J.; Belcher, W.; Dastoor, P.; et al. Low-Temperature CVD-Grown Graphene Thin Films as Transparent Electrode for Organic Photovoltaics. *Coatings* **2022**, *12*, 681. https://doi.org/10.3390/coatings12050681

Academic Editor: Sigitas Tamulevičius

Received: 29 March 2022
Accepted: 11 May 2022
Published: 16 May 2022

Publisher's Note: MDPI stays neutral with regard to jurisdictional claims in published maps and institutional affiliations.

Copyright: © 2022 by the authors. Licensee MDPI, Basel, Switzerland. This article is an open access article distributed under the terms and conditions of the Creative Commons Attribution (CC BY) license (https://creativecommons.org/licenses/by/4.0/).

1. Introduction

Graphene, a single layer, two-dimensional sheet of sp^2 hybridised carbon atoms arranged in a hexagonal lattice structure displays extraordinary electronic and thermal properties, unique optical properties and hardy mechanical strength [1–6]. These properties along with an abundance of carbon source material make graphene highly suited for replacing the scarce indium tin oxide (ITO) as a transparent electrode material for organic electronics [7–14]. Additionally, the application of graphene would eliminate degradation phenomena such as indium ion diffusion into the polymer layers of organic solar cells due to the intrinsic chemistry of ITO to acid/base conditions. Furthermore, the transparency of ITO is low at near-infrared regions wavelength and this affects the device efficiency of low bandgap materials. Furthermore, reduced transparency of ITO in near-infrared regions would cause a reduction in the device efficiency of low bandgap materials [15,16]. Chemical vapor deposition (CVD) has been a widely used tool for the fabrication of high-quality graphene on the surface of transition metal catalysts such as Co, Ni and especially Cu [17–21].

Cu foil is a promising catalyst for preparing CVD graphene due to its low carbon solubility, inexpensive metal cost and a high-degree of surficial self-limiting regime when

used for graphene synthesis [22]. Low-temperature growth (<1000 °C) of graphene layers in CVD is more economically desirable and feasible for industrial application [23]. The growth of graphene was demonstrated by coating poly(methyl methacrylate) (PMMA) or other solid hydrocarbon sources on copper substrates and subsequently heating above 800 °C to decompose the polymer [24]. The growth of graphene at low temperatures remains challenging, though the growth of graphene at a temperature as low as T_{growth} ~300 °C has been reported using liquid benzene as the hydrocarbon source; this procedure obtains high-quality monolayer graphene flakes [23]. More recently, Jaeho Kim et al. reported that a growth temperature below 400 °C can be achieved to obtain monolayer graphene with a few defects by forced convection of plasma-excited radicals [25]. Najmeh Koosha also reported that in the temperature range of 300–700 °C and using liquids such as methanol, N-butanol, N-heptane and cyclohexane, the quality of graphene structure can be improved [26].

A key aspect of enhancing the quality of polycrystalline CVD graphene is increasing the grain size of graphene domains via a very smooth surface of the catalyst. In 2011, Yu et al. prepared monolayer graphene single crystals on Cu, utilising Argon (Ar)-diluted methane (CH_4) as the carbon source with a grain size of ~15 μm [27]. Wu et al. fabricated ~1.2 mm sized monolayer graphene grains using solid carbon sources to trigger the growth on mechanically, electrochemically polished and atmospherically annealed copper foils [28]. The Ruoff group presented an improved method that can be used for the growth of large single-crystal graphene [29]. In this case, they reported the growth of ~2 mm single-crystal monolayer graphene grains inside of a Cu tube [29]. The graphene performance for photovoltaic and nano-electronic applications requires the removal of the catalytic metal substrate from graphene to apply the graphene film onto more suitable substrates. Polymer aided transfer has been used as a possible transfer technique. Using a wet and dry transfer method with polymer assistance including PMMA, polydimethylsiloxane (PDMS) frames or elastomer stamps have been demonstrated by several transfer processes. Transfer methods have been used as wet and dry transfer processes with polymer assistance such as film supporting PMMA and polydimethylsiloxane (PDMS) frames or elastomer stamps [30,31].

Compared to the exploration to improve the quality of graphene films, it is equally challenging in their applications to make working organic photovoltaic devices using graphene as the transparent electrode. High-temperature CVD grown graphene have been reported to be applied as the transparent conductive anode for organic photovoltaics (OPV) with structure graphene/poly (3,4-ethylene dioxythiophene):poly (styrene sulfonate) (PEDOT:PSS)/copper phthalocyanine (CuPc)/C60/bathocuproine(BCP)/Al. The sheet resistance (R_s) of the graphene electrode was 3.5 kΩ/□ at optical transmittance around 89% and achieved the power conversion efficiency (PCE) ~1.18% [9]. For another case, multilayers of graphene film as a cathode electrode in OPV structure of glass/ITO/ZnO/P3HT:PCBM/MLG was reported with the PCE of 2.5% [32]. However, if using a single layer of graphene (SLG) as the electrode, the device can be prepared with a sandwich structure of ITO/PEDOT/CuPC: C60: TPBi/SLG. The obtained device with a PCE was around ~0.22% [33]. These results indicated although graphene has the potential to be a new transparent electrode to replace the traditional ITO electrode, it is unlikely that this can be achieved with a single layer graphene film. A few other groups in the past ten years reported making organic solar cells using graphene multilayer thin films [34]. However, to our knowledge, those graphene thin films were grown at high temperature (1000 °C) CVD conditions.

Our group reported a study using PMMA as a matrix—trapped solvents can be used as the carbon source to grow graphene thin films. By carefully controlling the temperatures, a monolayer graphene can be grown by chemical vapor deposition at a growth temperature of 450 °C [35]. However, we found that it was almost impossible to successfully transfer those films.

In this study, we present a follow-up study and use a growth temperature (T_{growth}) of 600 °C. The obtained films still carry high quality graphene characteristics but with a

few more layers, which allows much easier transferring and further evaluation of their applications in the photovoltaic devices with more success.

2. Experimental Procedure

Graphene thin film was grown on Cu foils in an Atomate CVD system that consists of three heater coil zones and a gas flow controller. The Cu foil (2 cm × 1 cm) was electro-polished to reduce the roughness of the surface and to remove a surface coating layer applied by the manufacturer [29]. The Cu foil was then inserted into the CVD tube that is zone 2, and then the pumping system was started to evacuate the tube to a base pressure of 0.5 Torr and filled with Ar gas until it reached atmospheric pressure. After that, the CVD was heated to 900 °C for 1 h with a gas composition of H_2:Ar = 50:100 sccm which removed a native oxide layer and other contaminants from the surface of the Cu foil. The Cu foil was kept at elevated temperature for an hour to initiate grain growth. Afterwards, a 100 mg mL^{-1} PMMA solution in chlorobenzene was drop cast onto a quartz substrate and placed into zone 1 as a carbon source.

The carbon source was heated at 180 °C (T_{source}) to reveal carbon atoms onto the catalyst surface from the PMMA matrix. A temperature of 600 °C (T_{growth}) was utilised as the growth temperatures (catalyst temperatures) with an H_2:Ar (50:100 sccm) atmosphere in a 2-inch diameter quartz tube furnace of the CVD system. To prepare transparent electrodes from the prepared graphene films, the Cu foil had to be removed; this was carried out by polymer aided transfer. A wet transfer method with PMMA as polymer assistance was used for etching away the Cu in an aqueous iron nitrate ($Fe(NO_3)_3$) solution. PMMA (50 mg mL^{-1} in chlorobenzene) was spin-coated on top of the Cu foil and baked at 180 °C for 1 min. The Cu catalyst is then dissolved by chemical etching by $Fe(NO_3)_3$ (0.05 g mL^{-1}) throughout 48 h, resulting in floating PMMA/graphene films. The PMMA/graphene was washed with deionised (DI) water by picking it up using a clean glass substrate and transferring to a Petri dish containing DI water for 5 min. Subsequently, it was placed onto an arbitrary substrate and then dried. The transfer of graphene films is fundamentally inter-related and directly affects the performance of the film as a transparent electrode.

For device fabrication, on a transparent electrode (graphene or ITO)(ITO electrode: 15 Ω/□ ITO coated glass (XY15S); with a size 12.5 mm × 17.5 mm, XIN YAN technology limited), a 30 nm layer of poly(3,4-ethylene dioxythiophene-poly(styrene sulfonate) PEDOT:PSS (PVP AL4083 (purchased from Heraeus, Hanau, Germany) was deposited by spin coating and subsequently annealed at 140 °C for 30 min. P3HT: $PC_{61}BM$; synthesised at the University of Newcastle by Centro by organic electronics [36] (1:0.8) (200 nm) was spin-coated from chlorobenzene as photo-active layer following this evaporation of Ca (30 nm) and Al (120 nm). It was performed at 10^{-7} bar pressure (thermal evaporation; Angstrom Amod deposition system). A flow chart of the growth of graphene thin films, to film transferring and OPV device fabrication is depicted in Figure S1.

To better evaluation the quality of the graphene thin films, graphene films were transferred onto conductive silicon substrates in order to assess film morphology via scanning electron microscopy (SEM) (Zeiss Sigma VP SEM, Jena, Germany. The resolutions of this SEM were 1.3, 1.5 and 2.8 nm at operating voltages of 20, 15 and 1 kV, respectively. Additionally, atomic force microscopy (AFM) (Asylum Research Cypher AFM, Oxford Instruments, Abingdon, UK, tapping mode imaging in air, tap 300 Al-G) was used to investigate the morphology of the copper foil and graphene surface. Transmission electron microscopy (TEM) (Jeol, Tokyo, Japan was used to check the layers and crystallinity of the graphene thin film. TEM was performed on a Jeol 2100 with operating voltage of 80–200 kV and varying magnification ranges (10,000–100,000×). Graphene layers were suspended on copper grid substrates (GCu100, Pro Sci Tech, 100 mesh square) following the PMMA transfer method. A Renishaw inVia Raman spectroscopy with the laser excitation at 514 nm was used in this study for identifying the quality of graphene-based on the change in electron band. For Raman mapping, an XploRA PLUS Raman microscope from HORIBA Scientific (Kyoto, Japan, also with a 514 nm laser excitation, was used to check

the quality of graphene layers up to 100 × 100 μm^2 in dimensions. This instrument has a high-performance atomic force microscope (AFM) functionality with laser wavelength 532 nm (green), power 20 mW, NA 0.7 lens, spot size 400 nm and step size 1 nm. The transmission of graphene films transferred onto glass was measured on a Varian Cary 6000i UV-vis-NIR spectrophotometer (Agilent, Santa Clara, CA, USA). The work function of graphene films on silicon (Si) substrates was measured via UV photoelectron spectrometer (UPS) model AC-2, manufactured by Riken Keiki analysis (Tokyo, Japan). The model has a UV source with a unique electron detector that can operate at atmospheric pressure.

Electrical measurements determined the graphene thin-film-based device performances. A Keithley 2400 illuminated under a Newport class A solar simulator calibrated using a Si photo-diode measured the current density and voltage (J-V) curves of OPV devices. External quantum efficiency (EQE) of OPV devices were characterised using a tungsten halogen lamp passed through an Oriel Cornerstone 130 monochromator. This equipment measured the efficiency of OPV devices as a function with the energy of photon wavelength for determining the EQE. The impedance spectroscopy measurements were performed by LCR meter (Keysight E4980A, Santa Rosa, CA, USA) within the frequency range of 20–10^6 Hz under dark.

3. Results and Discussion

In an attempt to optimise the growth conditions for graphene thin films by CVD and subsequent transfer with more success, various temperatures (400, 500, 600, 700 and 800 °C) were applied in the growth phase. These films were characterised by Raman spectroscopy as shown in Figure 1. It can be seen (Table 1) that the most optimal G to 2D ratio was (0.50) found at a growth temperature of 600 °C under an H_2 flow rate of 50 sccm, whereas higher and lower temperatures lowered the ratio. H_2 gas flow rate has proven to be a significant parameter in the synthesis of graphene via CVD [37,38]. The influence of H_2 flow rate was also studied to improve the graphene film quality. Graphene films were deposited on Cu foil at a T_{growth} of 600 °C with a range of H_2 flow rates from 25 to 100 sccm [37]. The full peak width at half maximum (FWHM) of the 2D band of 53.37 cm^{-1} indicates good quality of graphene at T_{growth} of 600 °C with an H_2 flow rate of 75 sccm. Compared to other conditions of H_2 flow rate, the relative intensity ratio of G to a 2D band is an excellent 0.21, and this indicates a few layers of graphene for this growth condition (n GL~2) [39,40]. Graphene films grown at 600 °C with 75 sccm H_2 flow offered the highest successful rate of transferring, therefore, all graphene films used for OPV device fabrication were prepared under this condition. The scanning electron microscopy images in Figure S2 show the graphene film as grown on the copper foil and after transfer to a silicon substrate. The transferred graphene film is uniform, smooth and free of cracking. 2-D Raman mapping in Figure S3 illustrates that large grain of graphene domain can be formed in an area of 100 um × 100 um. However, uniformity is still a concern. With atomic force microscopy and transmission electron microscopy, film thickness of 2 (Figure S4) to tens of nanometres (Figure S5) were observed.

After transferring, the transmittance and resistance of graphene films were measured to determine the quality of each film for OPV devices applications. Figure 2a shows the relationship between the sheet resistance and optical transparency of CVD-grown graphene films. As illustrated in Figure 2a, the average sheet resistance of the graphene films was ~294 Ω/□ with optical transparency of ~65% at 500 nm, suggesting that these are ~15-layer graphene films (each layer absorbs 2.3% light). The variation in the sheet resistance of graphene film from 235 to 376 Ω/□ is likely due to the small domain size of the graphene attributed to the morphology of the Cu catalyst. Furthermore, undesirable impurities and defects in the transferred graphene films will cause a reduction in conductivity and transmission of graphene, where amorphous carbon exists between the graphene domains from the low-temperature growth process. A lower defect density of the graphene crystal lattice is expected to increase its conductivity as the defects in the lattice structure work as

scattering sites and block charge transport by limiting the mean free path of the conducting electrons [41].

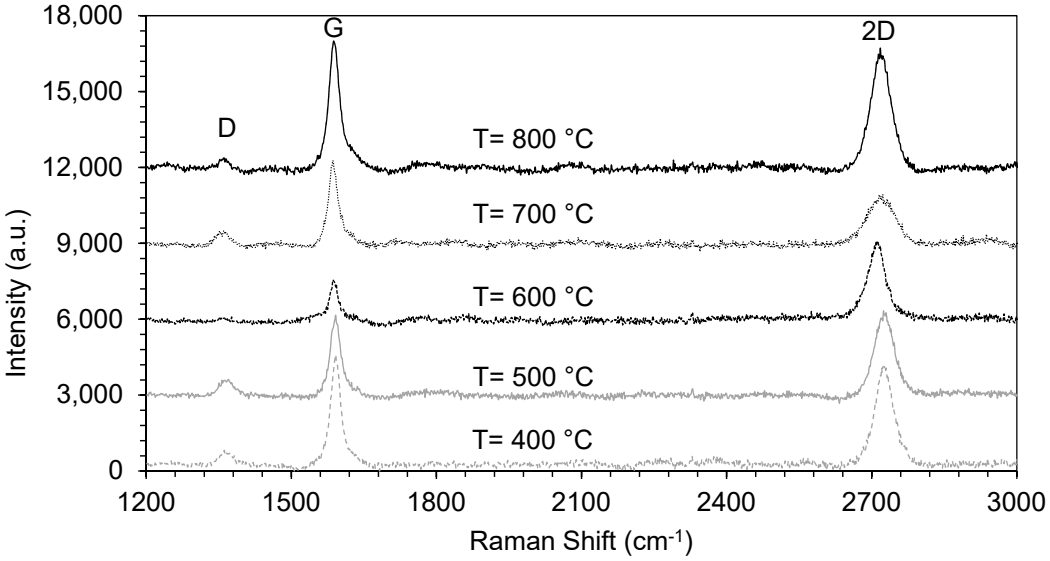


Figure 1. Raman spectra of graphene thin films grown with different growth temperatures. Spectra were collected when the graphene thin films were still on the copper foil surfaces.

Table 1. Characteristics value of Raman spectra regarding the G and 2D position, the intensity ratio between them and the $2D_{FWHM}$ are shown.

Growth Temperature (°C)	I_G/I_{2D}	$2D_{FWHM}$ (cm^{-1})
400	1.12	47.02
500	0.94	49.31
600	0.50	49.85
700	1.70	73.04
800	1.05	48.47

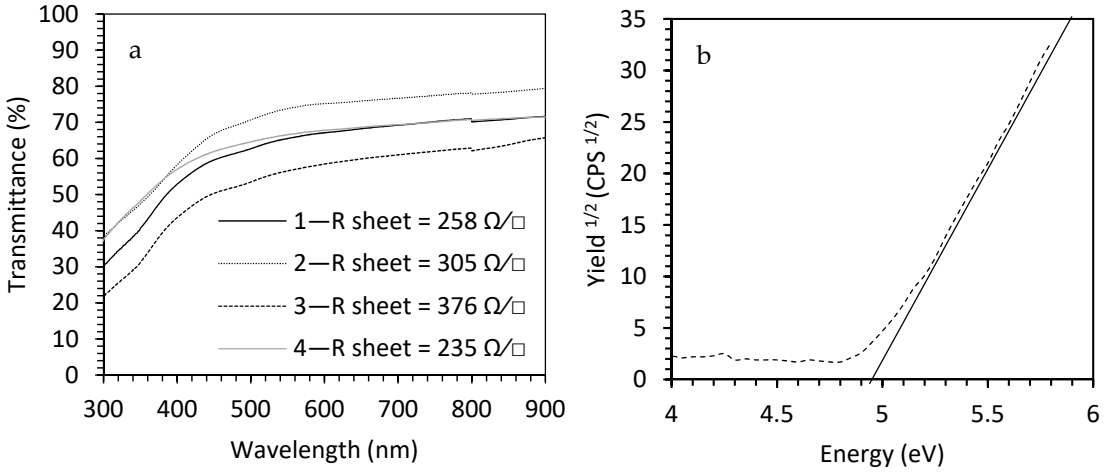


Figure 2. (**a**) Representative UV-Vis light transmission spectra for graphene thin films with sheet resistance (Ω/□). (**b**) Work function of graphene film transferred onto ITO-glass substrate.

Figure 2b shows the UPS spectrum of the work function of a graphene film on a silicon (Si) substrate where the graphene work function is calculated to be ~4.98 eV, while the work function of Si is ~4.67–4.92 eV [42]. The 4.65 eV work function of ITO [43] is sufficiently close that graphene film can be utilised as a replacement transparent electrode in organic

photovoltaics (OPVs), which has been done for both organic and dye-sensitised solar cells [9,44]. The modification of graphene's work function and sheet resistance (to more closely match that of ITO) could be a promising method for improving the performance of flexible organic light-emitting diodes (OLEDs) and OPV devices [45]. The work function of single-layer graphene has been reported to be in the range of 4.55–4.57 eV [46,47], with a separate report of 5.11 eV [48]. Besides, some experiments have shown the work function of monolayers graphene up to approximately 4.8 eV [49,50]. A change in Fermi level has been identified as the principal cause of a change in the work function value, where this Fermi level may be altered by doping with aromatic and gas molecules or ultraviolet irradiation [51,52]. Riedl et al. found that the substrate could affect the electronic properties of the graphene layer in a theoretical simulation [53], and this change was a function of the graphene film thickness, with an increase in work function with increasing the graphene film thickness [48]. Based on values of work function, this graphene film could be used as an alternative transparent electrode in OPVs for improving the band structure alignment at the interface layers of OPVs. The achievement of producing low-temperature graphene thin film electrodes is considered to be an excellent opportunity for the development of a new type of window electrode that is a flexible value of work function [54].

The graphene thin film electrode OPV is a new design for OPVs and will be compared to the performance and characteristics of standard ITO-electrode OPV devices in the conventional architecture. Consequently, both types of devices were fabricated using the same necessary procedure, and a graphene thin-film-based OPV with the architecture depicted in Figure 3 was produced. Graphene thin films (~2–20 nm) (shown in Figures S4 and S5) were transferred onto commercially available 0.7 mm thick glass substrates (XINYAN Technology Limited, XY15S) as the transparent anode, to which was added a low conductivity layer of poly(3,4-ethylene dioxythiophene-poly(styrene sulfonate) (PEDOT:PSS) as the hole transport layer (HTL). An active layer consists of blended poly (3-hexylthiophene-2,5-diyl) and phenyl-C_{61}-butyric acid methyl ester (P3HT:PCBM), calcium (Ca) layer as the electron transport layer (ETL) and aluminium (Al) as the back-electrode (cathode). ITO based devices were fabricated using the same procedure except that the glass substrate had a pre-patterned ITO electrode with a sheet resistance of 15 Ω/□ deposited on the glass slide. For the graphene devices, the layer of ITO was annihilated.

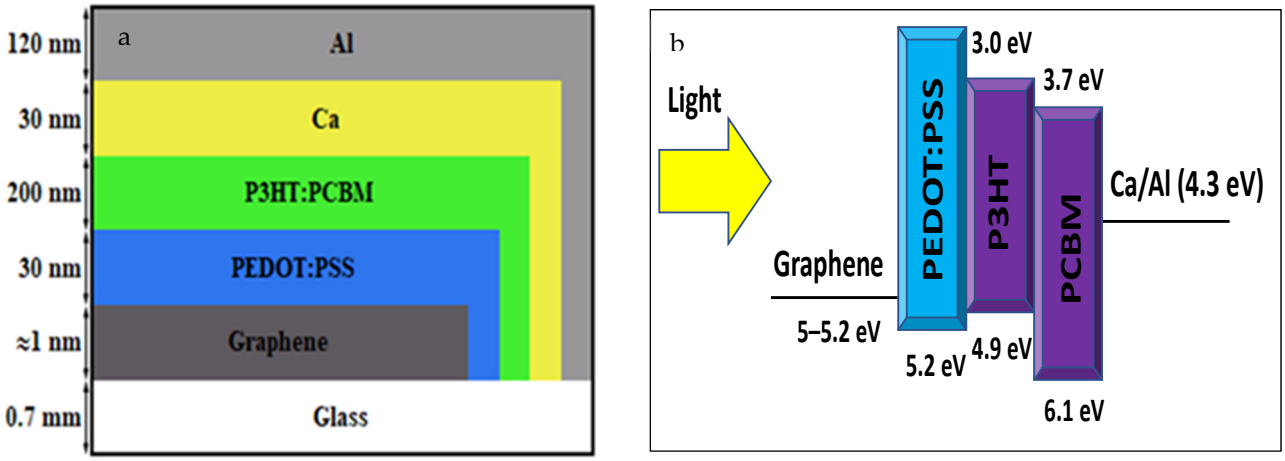


Figure 3. (**a**) The vertical architecture of an OPV device with a CVD graphene film as a transparent electrode (anode) and (**b**) the energy level diagram of graphene electrode in OPV.

The current density and voltages (J-V) characterisation of the device with the graphene electrode shows a J-V under dark conditions (mask area device 3.8 mm^2), as shown in Figure 4a. The linear, off-zero plot shows that the device is not acting as a diode but instead behaves as a resistor, suggesting that the graphene electrode is introducing a high resistance contact into the device. Under solar illumination, the OPV based on the graphene electrode

produced an open-circuit voltage (V_{oc}), short circuit current density (J_{sc}), fill factor (FF) and power conversion efficiency of 0.36 V, 4.28 mA/cm^2, 27% and 0.42%, respectively. Park et al. reported the promising attempt to use CVD-graphene which is grown at a high temperature of 1000 °C as window electrode. It was successful on organic photovoltaic (OPV) devices with power conversion efficiency (PCE) of 0.85% [11]. Moreover, CVD-graphene films grown at 1000 °C were utilised as a transparent anode electrode for OPVs with sheet resistance around 80 Ω/□ and transmittance 90%. The OPV structure was quartz/graphene/MoO_3 + PEDOT:PSS/P3HT:PCBM/LiF/Al and the outcome of PCE was ~2.5% [10]. In 2018, La Notte et al. prepared fully-sprayed flexible transparent OPVs via applying a high temperature CVD graphene electrode which was modified with cellulose additive by lamination process [55]. PCE of more than 3% was achieved in a single cell and almost 1% in mini-modules. Recently, graphene electrodes based on OPVs have obtained a very significant high PCE that supports this electrode being a promising material [56]. These results indicated the potential of graphene as a new transparent electrode for replacing the traditional ITO electrode. By contrast, the ITO-based device behaves as expected like a diode and has a much higher efficiency (Figure 4b). Device performance with the graphene transparent electrode was worse than that of the OPV based on ITO. The PCE is lower with the graphene film (0.42%) compared to that of devices with ITO (3.51%) at the mask area device.

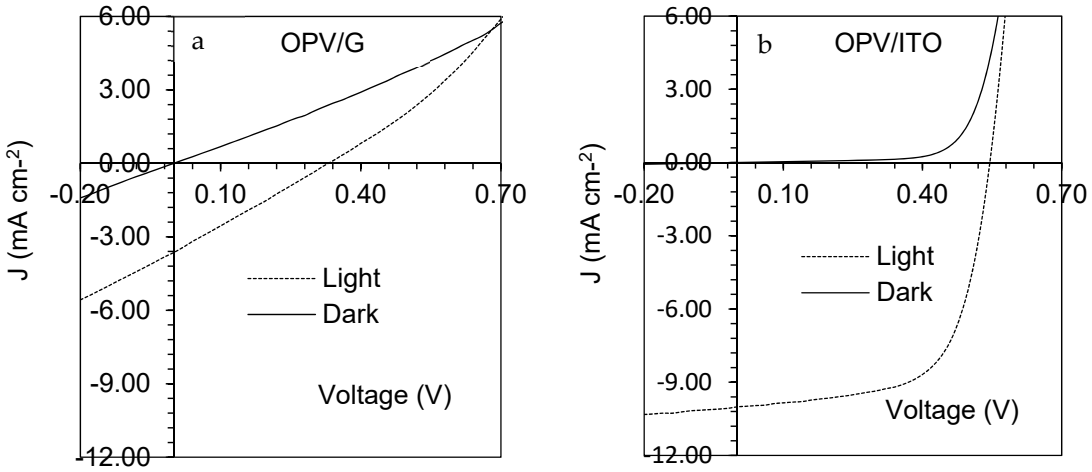


Figure 4. Current density–voltage (J-V) characteristics of OPV cells made from P3HT: $PC_{61}BM$ blend films, based on (**a**) graphene thin film and (**b**) ITO.

The PCE of standard devices which are based on ITO electrodes is considered a reasonable result comparing with previous work [57,58]. Besides, the hydrophobic nature of graphene makes the uniform coating of the PEDOT: PSS layer difficult and this may add to the issue [7]. Defects in the graphene electrode may also result in high recombination rate in the active layer, reducing the observed current density of the device. The OPV which is based on ITO has higher short-circuit current density (J_{sc}) (10 mA/cm^2) and open-circuit voltage (V_{oc}) (0.54 V) values than a graphene film-based device. Using graphene film as an anode electrode of OPV was fabricated by Xu et al. They prepared the structure of quartz/graphene/PEDOT: PSS/P3HT: PCBM/LiF/Al and obtained the PCE ~0.13% utilising large area production of graphene by a spin-coating method using graphene solutions [59]. In this work, there was a purpose of comparison that was testing using ITO as the electrode for OPV and the PCE of 3.517% was found [59]. In the cathode electrode environment, multilayers of graphene (MLG) film at a high-temperature growth have been used in OPV designed of MLG/WPF-6-oxy-F/P3HT: PCBM/PEDOT: PSS/Al. The PCE of these devices achieved about 1.23% [60].

The electrical and optical properties of graphene are degraded due to the transfer method, and this could lead to a reduction in its quality. Furthermore, one of most common

challenges for the integration of graphene electrodes into OPV devices is considered the incompatibility between the graphene electrode and the PEDOT: PSS hole transport layer (HTL) that increases the device failure rate [8]. Another reason for low J-V characterisation in OPV based on graphene can be the wrinkles and cracks which form in the graphene films due to the wet film transfer. This issue could result in discontinuities in charge transportation channels on the local scale of graphene domains in the electrode and would consequently decrease the efficiency of charge collection at the graphene electrode. Accordingly, the low level of performance in OPV based on graphene electrodes is concluded due to the high sheet resistance of the graphene electrode and morphological issues.

To illustrate how the ratio of the number of charge carriers collected by OPV based on CVD graphene compared to OPV based on ITO, we examined an external quantum efficiency (EQE) of OPVs based on both electrode materials. Figure 5 shows the EQE spectra for graphene and ITO electrode-based OPV devices. From this figure, it can be concluded that the number of photons which are converted to charge carriers in the active layer is decreased in OPV-graphene, at least in part because of low transparency (~65%) of graphene electrode. This measurement supports the hypothesis that graphene grown at low temperature and wet transferred onto a substrate does not result in a uniform film, and its morphology has been affected by transfer process. These issues can lead to an increase in the reflection of the graphene electrode and also cause a high sheet resistance with surface defects which create a leakage current and short circuit between the electrode and active layer through the PEDOT: PSS layer.

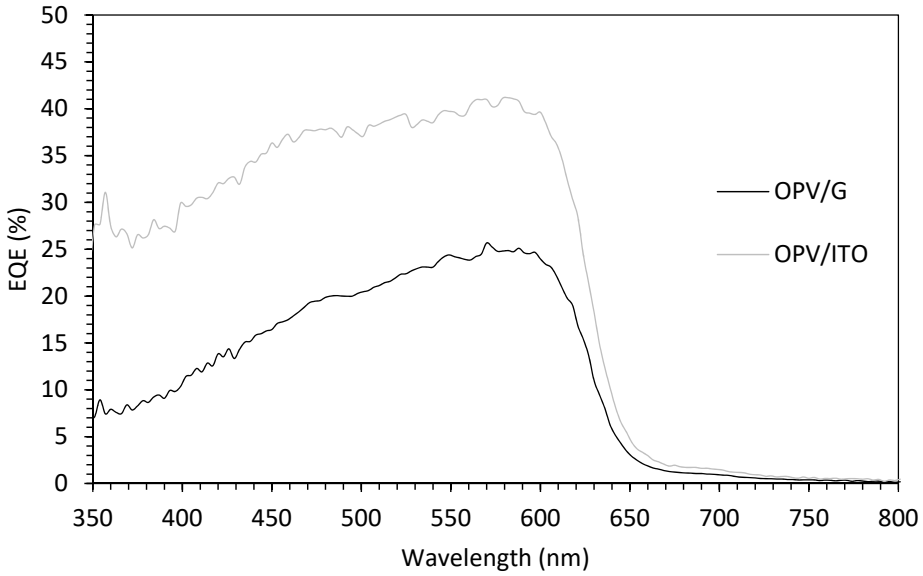


Figure 5. EQE spectra of OPV cells using graphene and ITO as a transparent electrode. This is for the best of five devices of OPV/G comparing with control standard device of OPV/ITO.

The device with an ITO transparent electrode has higher EQE across the entire wavelength range compared to the best of five devices based on graphene film as a window electrode. One factor contributing to a lower EQE is the higher optical absorption of the transparent electrode, compared to the ITO. Secondly, the difference in EQE can also be attributed to the efficiencies of charge collection and charge transfer at the graphene window electrode. EQE can be improved via reducing the number of graphene layers and obtaining a smoother surface (to prevent reflection and scattering of light), a challenge for transferred graphene films utilising the wet transfer method.

To further elucidate the effect of the graphene electrodes, the dark Nyquist plots of devices based on both ITO and prepared graphene electrodes are presented in Figure 6a,b. These plots give a complex plane representation of the imaginary part, Z'' of the impedance response versus its real part, Z'. These measurements are applied at different DC voltages

for covering the entire area where there is an effective operation of OPV (at range 0–6 V). It is noted that increasing of the applied voltage is responsible for connection to the recombination kinetics that occurred in the ITO device. Moreover, the low voltage region contributes to domination through the shunt resistance of device as a result of unavoidable leakage current which realises in the graphene device [61]. The overall impedance response includes a resistance connected in series R_0 that is ascribed to the ITO/graphene sheet and connecting wire contributions, and the results are practically frequency-independent [62,63]. It is shown that by considering the equivalent AC circuit as illustrated in Figure 6c, R_0 is higher for the graphene-based device and its value does not vary too much, whereas its value for the ITO-based device is less and increases continuously before dropping suddenly above 0.5 V. R_0 represents a series resistance which is attributed to the substrate and contacts of the device [64]. The circuit at the low-frequency region could be contacted to recombination resistance (R_{rec}) and the relaxation time is the free carrier lifetime of OPV (R_1, C_1) [64]. The capacity (C_1) from this device is associated with chemical capacitance ($C\mu$). This capacitance could be increased via charge and carrier density with a change in the Fermi-level [64,65]. These results imply an ohmic contact of graphene (meaning that it acts as a resistor and poorly collects charge) and a more rectifying behaviour, as expected, for ITO substrate.

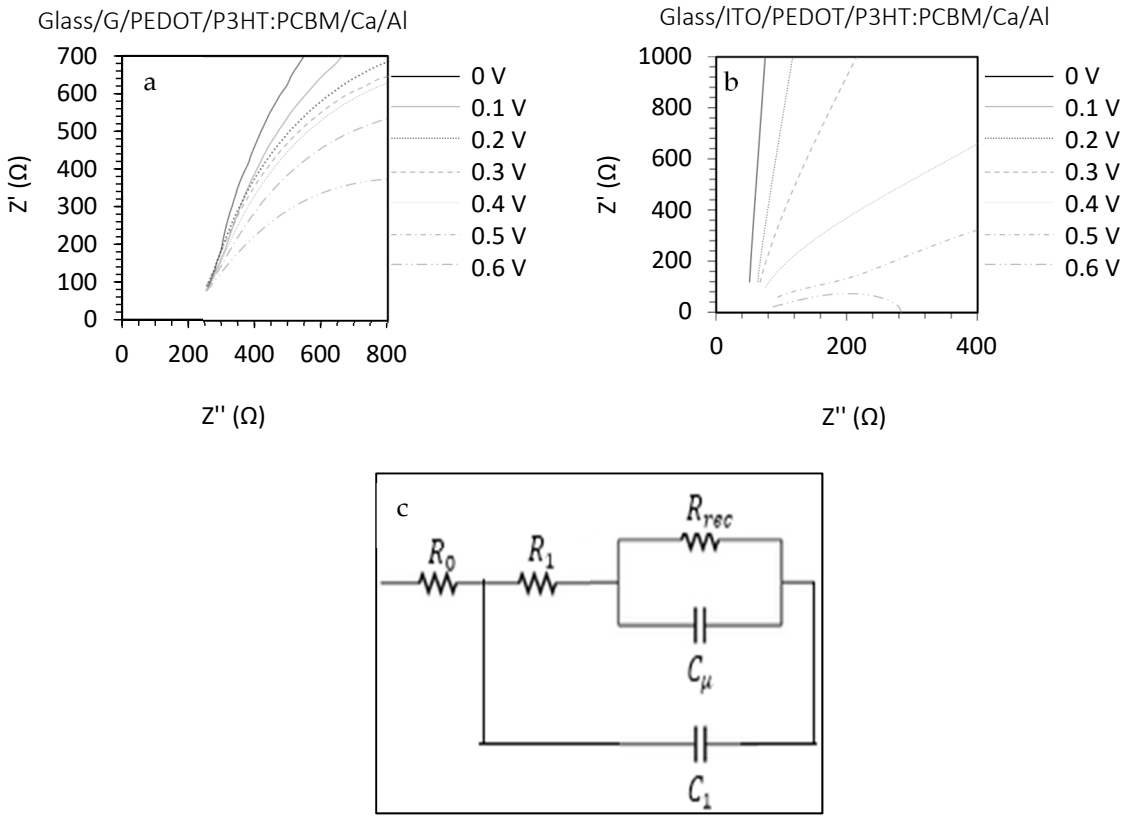


Figure 6. Nyquist plots of OPV devices is based on (**a**) graphene and (**b**) ITO as a transparent electrode, (**c**) the equivalent AC circuit of OPV.

Detailed analysis for the two electrodes (graphene and ITO) is presented in Figure 7a, where the frequency responses of the real part of the OPV impedance are displayed on a linear scale. The voltage bias for this analysis was applied from 0.1 to 0.4 V, and the real part of the impedance was plotted versus the frequency. At the higher frequency range, the resistance part of the impedance showed similar dropping values for both devices. Figure 7b shows the device resistance as a function of bias voltage. The real resistance of the OPV based on graphene electrode is higher (206 Ω) compared with the ITO electrode ~(50–70 Ω). The analysis viewed the changing of real part resistance as narrow

and wide region vs. frequency of ITO and graphene devices. This realised a narrow area of real resistance in graphene OPV, but it was a wider region in ITO OPV. It is considered as an influence of the high resistance electrode on the device and contributed to the real part resistance in the impendency. Moreover, the defect in graphene electrode could be limited to block the moving of transport charger and carrier density through OPV. This contributes a huge effect on the combination mechanism [61]. The higher sheet resistance of the graphene electrode is therefore directly reflected in the overall resistance of devices, reducing the device performance. The real part resistance was reduced constantly via increasing the bias voltage that is related to the dropped resistance with a higher voltage at the low region of frequency. These results are also reflected in the dark J-V curves, where a linear J vs. V plot gives a constant resistance for the graphene-based device, but a non-ohmic contact is observed for the ITO-based OPV device as shown in Figure 7b.

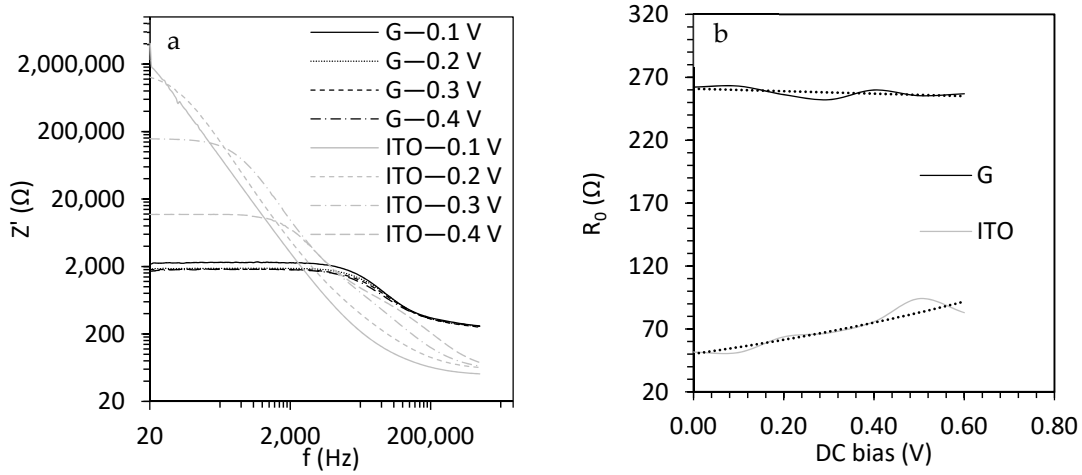


Figure 7. (**a**) Dispersion of total real part resistance of impedance versus frequency for OPVs based on graphene and ITO as window electrodes, and (**b**) the linear J variations vs. V for graphene-based device, and ITO-based OPV device.

To investigate the practicality of area dependence of using graphene films as window electrodes in OPV devices, various areas of graphene devices were fabricated and illuminated under masks of varying sizes. This experiment was undertaken to determine the viability of low-temperature graphene electrodes for electronic applications. Initially in this study, devices with an active area of 5 mm^2 were prepared and their performances were characterised under full illumination and the standard mask area of 3.8 mm^2. Typical J-V curves are shown in Figure 8. This figure shows an obvious effect of changing the illuminated area of the graphene electrode on the performance of the OPV. For full area illumination of the device (5 mm^2), an open-circuit voltage (V_{oc}) of 0.5 V, a short-circuit current density (J_{sc}) of 8.48 mA/cm^2, an FF of 29% and an efficiency (PCE) of 1.27% is observed. This is the highest efficiency observed for these devices. However, upon applying a mask to the device the performance of the device drops. Under the 3.8 mm^2 mask, the device achieved lower values for V_{oc}, J_{sc}, FF and PCE of 0.37 V, 3.91 mA/cm^2, 27% and 0.39%, respectively. The reduction in J_{sc} is to be expected but the reductions in V_{oc}, FF and especially PCE are surprising and is counter to what might be expected.

The reduction in the OPVs performance with an illuminated area could be related to an increase in the density of contamination on the graphene surface. To further probe the influence of scale area electrodes on the performance of OPVs based on graphene films, the graphene area electrode was optimized at areas of full device illumination, 5 mm^2, and with mask areas of 3.8, 3 and 2 mm^2. There is a steady and systematic improvement in device performance as the area of the mask increases from 2 to 5 mm^2 (Figure 9). The devices improve from ~0.2% with the 2 mm^2 masks to >1% for the 5 mm^2 devices. This improvement is a function of both the J_{sc} and V_{oc} of the device, both of which also

systematically improve, whilst FF remains constant (Table 2). This observed improvement in device performance with device area is counter to what might be expected and can only be explained in terms of charge trap states in the graphene electrode [66].

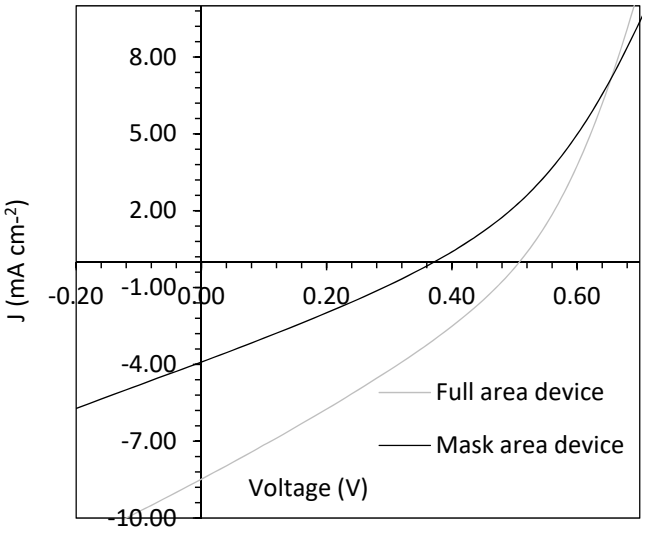


Figure 8. J-V characterisation of OPV based on graphene electrode when illuminated under the full area and the mask area.

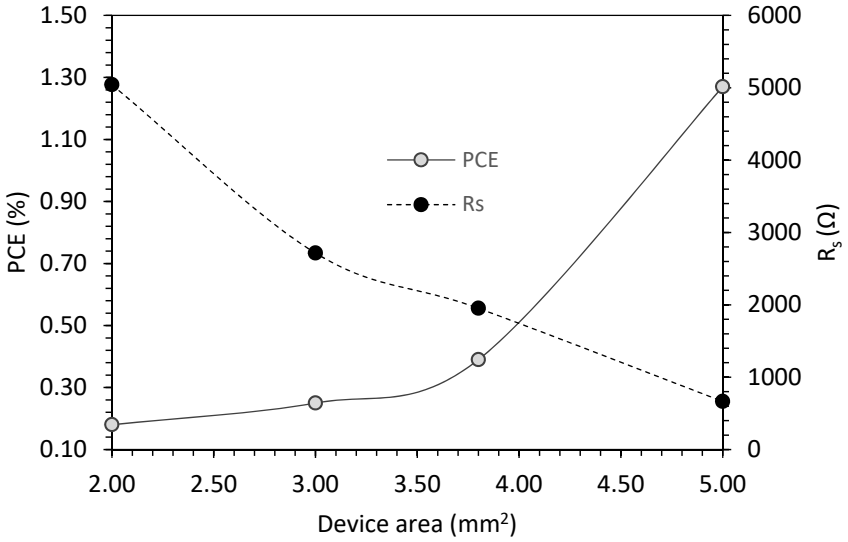


Figure 9. Diagram relationship between PCE of OPVs based on graphene electrodes and scale areas devices.

Table 2. J-V analysis of OPV based on graphene electrode at different areas.

Device Type	PCE (%)	V_{oc} (V)	J_{sc} (mA/cm^2)	Fill Factor	Cell Area (mm^2)
OPV/G	0.18	0.27	2.58	0.25	2
OPV/G	0.25	0.29	3.28	0.25	3
OPV/G	0.39	0.37	3.91	0.27	3.8
OPV/G	1.27	0.5	8.48	0.29	5

Figure 9 shows the series resistance (R_s) of the device as a function of the mask area. The Rs shows an inverse relationship with the PCE of the devices, systematically decreasing as the area of illumination increases. Increasing the area of illumination on the graphene electrode OPV appears to improve the conductivity of the electrode. This could be a result

of two factors. The distance between the average site of exciton generation in the active layer and the contact point on the substrate is reduced by increasing the illuminated area, effectively reducing the average charge pathway through the graphene.

We have established that defects and contamination reduce the conductivity of the graphene electrode. These defects result in charge trapping and lower the conductivity, reducing device performance. When the device is illuminated these charge traps are initially filled. Once this has happened, subsequent charges are free to travel through the graphene, resulting in increased photoconductivity of the graphene in contact with the active layer. As the illuminated region is increased in size, the overall conductivity of the graphene electrode is increased and the device performance increases. V_{oc} also increases since, when the traps are filled, recombination due to these traps is eliminated. Thus, counterintuitively, increasing the mask area results in a direct and systematic increase in device efficiency. This is a result which interestingly suggests that large area graphene electrode-based OPVs are maybe more viable that small area devices. As shown in Table S1, our overall device performance is comparable to the devices reported in the literature with similar structures [67–70].

4. Conclusions

Preparation of CVD graphene at low temperature is still a difficulty for obtaining a high-quality electrode compared with ITO. The conductivity of graphene was lower than ITO due to small domains size of graphene and defects from the transfer method. The temperature growth affected the quality of graphene electrodes, which is identified from Raman data. The graphene electrode was prepared at 600 °C with 75 sccm of H_2 flow. Subsequently, the understanding of low-temperature graphene-based OPV devices and investigating the polymer formation on these graphene surfaces are of great interest to create a new way of preparing environmental and economical conductive electrodes. The morphology, structure, and optical properties of graphene films were characterised using AFM SEM, TEM and Raman spectroscopy and it was found that multilayer graphene was formed with amorphous carbon present and that the transfer technique resulted in tears, folding and wrinkles in the graphene electrode. The studies of J-V data for these OPV devices based on graphene have demonstrated that the small graphene flakes produced by low-temperature growth and the morphological defects resulting from the transfer method limit device performance. A large area device of 1.27% efficiency was achieved and methodology for preparing the optically transparent, large area, low-temperature graphene electrodes presented. This work provides the basis for a promising procedure for applying graphene grown at low temperature to industry applications.

Supplementary Materials: The following supporting information can be downloaded at: https://www.mdpi.com/article/10.3390/coatings12050681/s1, Figure S1: A flow chart of the entire process from the preparation of graphene thin film electrode to OPV device fabrication; Figure S2: Scanning electron microscopy images of graphene film (a) on the copper foil surface and (b) after transferring to a silicon substrate. The film was grown at T_{growth} 600 °C for 1 min with H_2 = 75 sccm; Figure S3: (a) A spatial map of a graphene film using Raman G/2D peak ratio over a 100 × 100 μm area and (b) Raman 2D peak mapping at the same area. The film was grown at T_{growth} 600 °C with a H_2 flow rate at 75 sccm; Figure S4: Atomic force microscopy image of a graphene film transferred onto a silicon substrate. The insert shows the thickness around 2 nm of the graphene film; Figure S5: (a) Transmission electron microscopy image of graphene multi-layers folded at the edge of film and, (b) Electronic diffraction of graphene layers suspended on Cu grid at a selected area; Table S1: A summary of device performance of organic solar cells using a graphene thin film as the transparent electrode, with a P3HT/PCBM bulk heterojunction active layer reported in the literature. Graphene thin films were all grown using chemical vapor deposition.

Author Contributions: Conceptualization and Supervision, X.Z., P.D., W.B. and J.H.; Investigation, A.Y.A., N.P.H., K.F., M.N.T. and M.A.; Resources, M.G.B. and A.F.; Writing—original draft preparation, A.Y.A. and N.P.H.; Writing—review and editing, N.P.H., W.B., P.D. and X.Z. All authors have read and agreed to the published version of the manuscript.

Funding: This research received no external funding.

Institutional Review Board Statement: Not applicable.

Informed Consent Statement: Not applicable.

Data Availability Statement: Not applicable.

Acknowledgments: The researchers gratefully acknowledge the financial support for this work from the Centre for Organic Electronics at the University of Newcastle, and Alaa Y. Ali would also like to thank the Higher Committee for Education Development in Iraq (HCED-Iraq) for supporting his PhD scholarship. This project was performed in part at the Material's Node of the Australian National Fabrication Facility (ANFF), which is a company established under the National Collaborative Research Infrastructure Strategy to provide nano- and micro-fabrication facilities for Australia's researchers. Special thanks to the University of Newcastle Electron Microscopy and X-ray Unit.

Conflicts of Interest: The authors declare no conflict of interest.

References

1. Geim, A.K.; Novoselov, K.S. The rise of graphene. *Nat. Mater.* **2007**, *6*, 183–191. [CrossRef] [PubMed]
2. Castro Neto, A.H.; Peres, N.M.R.; Novoselov, K.S.; Geim, A.K. The electronic properties of graphene. *Rev. Mod. Phys.* **2009**, *81*, 109–162. [CrossRef]
3. Novoselov, K.S.; Geim, A.K.; Morozov, S.V.; Jiang, D.; Zhang, Y.; Dubonos, S.V.; Grigorieva, I.V.; Firsov, A.A. Electric field effect in atomically thin carbon films. *Science* **2004**, *306*, 666–669. [CrossRef] [PubMed]
4. Balandin, A.A.; Ghosh, S.; Bao, W.; Calizo, I.; Teweldebrhan, D.; Miao, F.; Lau, C.N. Superior thermal conductivity of single-layer graphene. *Nano Lett.* **2008**, *8*, 902–907. [CrossRef] [PubMed]
5. Lee, C.; Wei, X.; Kysar, J.W.; Hone, J. Measurement of the elastic properties and intrinsic strength of monolayer graphene. *Science* **2008**, *321*, 385–388. [CrossRef] [PubMed]
6. Nair, R.R.; Blake, P.; Grigorenko, A.N.; Novoselov, K.S.; Booth, T.J.; Stauber, T.; Peres, N.M.; Geim, A.K. Fine structure constant defines visual transparency of graphene. *Science* **2008**, *320*, 1308. [CrossRef] [PubMed]
7. Wang, Y.; Chen, X.; Zhong, Y.; Zhu, F.; Loh, K.P. Large area, continuous, few-layered graphene as anodes in organic photovoltaic devices. *Appl. Phys. Lett.* **2009**, *95*, 063302. [CrossRef]
8. Hyesung, P.; Jill, A.R.; Ki Kang, K.; Vladimir, B.; Jing, K. Doped graphene electrodes for organic solar cells. *Nanotechnology* **2010**, *21*, 505204.
9. Gomez De Arco, L.; Zhang, Y.; Schlenker, C.W.; Ryu, K.; Thompson, M.E.; Zhou, C. Continuous, highly flexible, and transparent graphene films by chemical vapor deposition for organic photovoltaics. *ACS Nano* **2010**, *4*, 2865–2873. [CrossRef]
10. Wang, Y.; Tong, S.W.; Xu, X.F.; Özyilmaz, B.; Loh, K.P. Interface engineering of layer-by-layer stacked graphene anodes for high-performance organic solar cells. *Adv. Mater.* **2011**, *23*, 1514–1518. [CrossRef]
11. Park, H.; Brown, P.R.; Bulović, V.; Kong, J. Graphene as transparent conducting electrodes in organic photovoltaics: Studies in graphene morphology, hole transporting layers, and counter electrodes. *Nano Lett.* **2012**, *12*, 133–140. [CrossRef] [PubMed]
12. Zhang, Q.; Wan, X.; Xing, F.; Huang, L.; Long, G.; Yi, N.; Ni, W.; Liu, Z.; Tian, J.; Chen, Y. Solution-processable graphene mesh transparent electrodes for organic solar cells. *Nano Res.* **2013**, *6*, 478–484. [CrossRef]
13. Park, H.; Chang, S.; Smith, M.; Gradečak, S.; Kong, J. Interface engineering of graphene for universal applications as both anode and cathode in organic photovoltaics. *Sci. Rep.* **2013**, *3*, 1581. [CrossRef] [PubMed]
14. Hobeom, K.; Sang-Hoon, B.; Tae-Hee, H.; Kyung-Geun, L.; Jong-Hyun, A.; Tae-Woo, L. Organic solar cells using CVD-grown graphene electrodes. *Nanotechnology* **2014**, *25*, 014012.
15. Wang, X.; Zhi, L.; Müllen, K. Transparent, conductive graphene electrodes for dye-sensitized solar cells. *Nano Lett.* **2008**, *8*, 323–327. [CrossRef]
16. Wang, X.; Zhi, L.; Tsao, N.; Tomovic, Z.; Li, J.; Mullen, K. Transparent carbon films as electrodes in organic solar cells. *Angew. Chem. Int. Ed. Engl.* **2008**, *47*, 2990–2992. [CrossRef]
17. Li, X.; Cai, W.; An, J.; Kim, S.; Nah, J.; Yang, D.; Piner, R.; Velamakanni, A.; Jung, I.; Tutuc, E.; et al. Large-area synthesis of high-quality and uniform graphene films on copper foils. *Science* **2009**, *324*, 1312–1314. [CrossRef]
18. Bae, S.; Kim, H.; Lee, Y.; Xu, X.; Park, J.-S.; Zheng, Y.; Balakrishnan, J.; Lei, T.; Ri Kim, H.; Song, Y.I.; et al. Roll-to-roll production of 30-inch graphene films for transparent electrodes. *Nat. Nanotechnol.* **2010**, *5*, 574–578. [CrossRef]
19. Kim, K.S.; Zhao, Y.; Jang, H.; Lee, S.Y.; Kim, J.M.; Kim, K.S.; Ahn, J.H.; Kim, P.; Choi, J.Y.; Hong, B.H. Large-scale pattern growth of graphene films for stretchable transparent electrodes. *Nature* **2009**, *457*, 706–710. [CrossRef]
20. Reina, A.; Jia, X.; Ho, J.; Nezich, D.; Son, H.; Bulovic, V.; Dresselhaus, M.S.; Kong, J. Large area, few-layer graphene films on arbitrary substrates by chemical vapor deposition. *Nano Lett.* **2009**, *9*, 30–35. [CrossRef]
21. Ago, H.; Ito, Y.; Mizuta, N.; Yoshida, K.; Hu, B.; Orofeo, C.M.; Tsuji, M.; Ikeda, K.-I.; Mizuno, S. Epitaxial chemical vapor deposition growth of single-layer graphene over cobalt film crystallized on sapphire. *ACS Nano* **2010**, *4*, 7407–7414. [CrossRef] [PubMed]

22. Miyata, Y.; Kamon, K.; Ohashi, K.; Kitaura, R.; Yoshimura, M.; Shinohara, H. A simple alcohol-chemical vapor deposition synthesis of single-layer graphenes using flash cooling. *Appl. Phys. Lett.* **2010**, *96*, 263105. [CrossRef]
23. Li, Z.; Wu, P.; Wang, C.; Fan, X.; Zhang, W.; Zhai, X.; Zeng, C.; Li, Z.; Yang, J.; Hou, J. Low-temperature growth of graphene by chemical vapor deposition using solid and liquid carbon sources. *ACS Nano* **2011**, *5*, 3385–3390. [CrossRef] [PubMed]
24. Sun, Z.; Yan, Z.; Yao, J.; Beitler, E.; Zhu, Y.; Tour, J.M. Growth of graphene from solid carbon sources. *Nature* **2010**, *468*, 549–552. [CrossRef] [PubMed]
25. Jaeho Kim, H.S.; Itagaki, H. Low-temperature graphene growth by forced convection of plasma-excited radi-cals. *Nano Lett.* **2019**, *19*, 739–746.
26. Koosha, N.; Karimi-Sabet, J.; Moosavian, M.A.; Amini, Y. Improvement of synthesized graphene structure through various solvent liquids at low temperature by chemical vapor deposition method. *Mater. Sci. Eng. B* **2021**, *274*, 115458. [CrossRef]
27. Yu, Q.; Jauregui, L.A.; Wu, W.; Colby, R.; Tian, J.; Su, Z.; Cao, H.; Liu, Z.; Pandey, D.; Wei, D.; et al. Control and characterization of individual grains and grain boundaries in graphene grown by chemical vapour deposition. *Nat. Mater.* **2011**, *10*, 443–449. [CrossRef]
28. Wu, T.; Ding, G.; Shen, H.; Wang, H.; Sun, L.; Jiang, D.; Xie, X.; Jiang, M. Triggering the continuous growth of graphene toward millimeter-sized grains. *Adv. Funct. Mater.* **2013**, *23*, 198–203. [CrossRef]
29. Chen, S.; Ji, H.; Chou, H.; Li, Q.; Li, H.; Suk, J.W.; Piner, R.; Liao, L.; Cai, W.; Ruoff, R.S. Millimeter-size single-crystal graphene by suppressing evaporative loss of cu during low pressure chemical vapor deposition. *Adv. Mater.* **2013**, *25*, 2062–2065. [CrossRef]
30. Suk, J.W.; Kitt, A.; Magnuson, C.W.; Hao, Y.; Ahmed, S.; An, J.; Swan, A.K.; Goldberg, B.B.; Ruoff, R.S. Transfer of CVD-grown monolayer graphene onto arbitrary substrates. *ACS Nano* **2011**, *5*, 6916–6924. [CrossRef]
31. Song, J.; Kam, F.-Y.; Png, R.-Q.; Seah, W.-L.; Zhuo, J.-M.; Lim, G.-K.; Ho, P.K.H.; Chua, L.-L. A general method for transferring graphene onto soft surfaces. *Nat. Nanotechnol.* **2013**, *8*, 356–362. [CrossRef] [PubMed]
32. Lee, Y.-Y.; Tu, K.-H.; Yu, C.-C.; Li, S.-S.; Hwang, J.-Y.; Lin, C.-C.; Chen, K.-H.; Chen, L.-C.; Chen, H.-L.; Chen, C.-W. Top laminated graphene electrode in a semitransparent polymer solar cell by simultaneous thermal annealing/releasing method. *ACS Nano* **2011**, *5*, 6564–6570. [CrossRef] [PubMed]
33. Cox, M.; Gorodetsky, A.; Kim, B.; Kim, K.S.; Jia, Z.; Kim, P.; Nuckolls, C.; Kymissis, I. Single-layer graphene cathodes for organic photovoltaics. *Appl. Phys. Lett.* **2011**, *98*, 123303. [CrossRef]
34. Rosli, N.N.; Ibrahim, M.A.; Ludin, N.A.; Teridi, M.A.M.; Sopian, K. A review of graphene based transparent conducting films for use in solar photovoltaic applications. *Renew. Sustain. Energy Rev.* **2019**, *99*, 83. [CrossRef]
35. Sulaiman, K.; Ali, A.Y.; Elkington, D.; Feron, K.; Anderson, K.F.; Belcher, W.; Dastoor, P.; Zhou, X. Matrix assisted low temperature growth of graphene. *Carbon* **2016**, *107*, 325–331. [CrossRef]
36. Cooling, N.A.; Barnes, E.F.; Almyahi, F.; Feron, K.; Al-Mudhaffer, M.F.; Al-Ahmad, A.; Vaughan, B.; Andersen, T.R.; Griffith, M.J.; Hart, A.S.; et al. A low-cost mixed fullerene acceptor blend for printed electronics. *J. Mater. Chem. A* **2016**, *4*, 10274–10281. [CrossRef]
37. Ali, A.Y.; Holmes, N.P.; Holdsworth, J.; Belcher, W.; Dastoor, P.; Zhou, X. Growth of multi-layered graphene using organic solvent-pmma film as the carbon source under low temperature conditions. *Int. J. Chem. Mater. Eng.* **2019**, *13*, 77–81.
38. Losurdo, M.; Giangregorio, M.M.; Capezzuto, P.; Bruno, G. Graphene CVD growth on copper and nickel: Role of hydrogen in kinetics and structure. *Phys. Chem. Chem. Phys.* **2011**, *13*, 20836–20843. [CrossRef]
39. Wu, W.; Yu, Q.; Peng, P.; Liu, Z.; Bao, J.; Pei, S.S. Control of thickness uniformity and grain size in graphene films for transparent conductive electrodes. *Nanotechnology* **2012**, *23*, 035603. [CrossRef]
40. Das, A.; Chakraborty, B.; Sood, A.K. Raman spectroscopy of graphene on different substrates and influence of defects. *Bull Mater. Sci.* **2008**, *31*, 579–584. [CrossRef]
41. Singh, V.; Joung, D.; Zhai, L.; Das, S.; Khondaker, S.I.; Seal, S. Graphene based materials: Past, present and future. *Prog. Mater. Sci.* **2011**, *56*, 1178–1271. [CrossRef]
42. Dillon, J.A., Jr.; Farnsworth, H.E. work function and sorption properties of silicon crystals. *J. Appl. Phys.* **1958**, *29*, 1195–1202. [CrossRef]
43. Wu, J.; Becerril, H.A.; Bao, Z.; Liu, Z.; Chen, Y.; Peumans, P. Organic solar cells with solution-processed graphene transparent electrodes. *Appl. Phys. Lett.* **2008**, *92*, 263302. [CrossRef]
44. Lee, K.S.; Lee, Y.; Lee, J.Y.; Ahn, J.-H.; Park, J.H. Flexible and platinum-free dye-sensitized solar cells with conducting-polymer-coated graphene counter electrodes. *ChemSusChem* **2012**, *5*, 379–382. [CrossRef] [PubMed]
45. Han, T.-H.; Lee, Y.; Choi, M.-R.; Woo, S.-H.; Bae, S.-H.; Hong, B.H.; Ahn, J.-H.; Lee, T.-W. Extremely efficient flexible organic light-emitting diodes with modified graphene anode. *Nat. Photonics* **2012**, *6*, 105–110. [CrossRef]
46. Yu, Y.-J.; Zhao, Y.; Ryu, S.; Brus, L.E.; Kim, K.S.; Kim, P. Tuning the graphene work function by electric field effect. *Nano Lett.* **2009**, *9*, 3430–3434. [CrossRef]
47. Bußmann, B.K.; Ochedowski, O.; Schleberger, M. Doping of graphene exfoliated on $SrTiO_3$. *Nanotechnology* **2011**, *22*, 265703. [CrossRef]
48. Mattausch, A.; Pankratov, O. Ab initio study of graphene on SiC. *Phys. Rev. Lett.* **2007**, *99*, 076802. [CrossRef]
49. Yan, R.; Zhang, Q.; Li, W.; Calizo, I.; Shen, T.; Richter, C.A.; Hight-Walker, A.R.; Liang, X.; Seabaugh, A.; Jena, D.; et al. Determination of graphene work function and graphene-insulator-semiconductor band alignment by internal photoemission spectroscopy. *Appl. Phys. Lett.* **2012**, *101*, 022105. [CrossRef]

50. Shi, Y.; Kim, K.K.; Reina, A.; Hofmann, M.; Li, L.-J.; Kong, J. Work function engineering of graphene electrode via chemical doping. *ACS Nano* **2010**, *4*, 2689–2694. [CrossRef]
51. Dong, X.; Fu, D.; Fang, W.; Shi, Y.; Chen, P.; Li, L.-J. Doping single-layer graphene with aromatic molecules. *Small* **2009**, *5*, 1422–1426. [CrossRef] [PubMed]
52. Lin, Y.-J.; Zeng, J.-J. Tuning the work function of graphene by ultraviolet irradiation. *Appl. Phys. Lett.* **2013**, *102*, 183120. [CrossRef]
53. Riedl, C.; Coletti, C.; Starke, U. Structural and electronic properties of epitaxial graphene on SiC(0 0 0 1): A review of growth, characterization, transfer doping and hydrogen intercalation. *J. Phys. D Appl. Phys.* **2010**, *43*, 374009. [CrossRef]
54. Yang, N.; Yang, D.; Chen, L.; Liu, D.; Cai, M.; Fan, X. Design and adjustment of the graphene work function via size, modification, defects, and doping: A first-principle theory study. *Nanoscale Res. Lett.* **2017**, *12*, 642. [CrossRef] [PubMed]
55. La Notte, L.; Bianco, G.V.; Palma, A.L.; Di Carlo, A.; Bruno, G.; Reale, A. Sprayed organic photovoltaic cells and mini-modules based on chemical vapor deposited graphene as transparent conductive electrode. *Carbon* **2018**, *129*, 878–883. [CrossRef]
56. Koo, D.J.; Jung, S.; Seo, J.; Jeong, G.; Choi, Y.; Lee, J.; Oh, J.; Yang, C.; Park, H. Flexible organic solar cells over 15% efficiency with polyimide-integrated graphene electrodes. *Joule* **2020**, *4*, 1021–1034. [CrossRef]
57. Chi, D.; Qu, S.; Wang, Z.; Wang, J. High efficiency P3HT:PCBM solar cells with an inserted PCBM layer. *J. Mater. Chem. C* **2014**, *2*, 4383–4387. [CrossRef]
58. Chen, L.-M.; Hong, Z.; Li, G.; Yang, Y. Recent progress in polymer solar cells: Manipulation of polymer:fullerene morphology and the formation of efficient inverted polymer solar cells. *Adv. Mater.* **2009**, *21*, 1434–1449. [CrossRef]
59. Xu, Y.; Long, G.; Huang, L.; Huang, Y.; Wan, X.; Ma, Y.; Chen, Y. Polymer photovoltaic devices with transparent graphene electrodes produced by spin-casting. *Carbon* **2010**, *48*, 3308–3311. [CrossRef]
60. Jo, G.; Na, S.-I.; Oh, S.-H.; Lee, S.; Kim, T.-S.; Wang, G.; Choe, M.; Park, W.; Yoon, J.; Kim, D.-Y.; et al. Tuning of a graphene-electrode work function to enhance the efficiency of organic bulk heterojunction photovoltaic cells with an inverted structure. *Appl. Phys. Lett.* **2010**, *97*, 213301. [CrossRef]
61. Garcia-Belmonte, G.; Guerrero, A.; Bisquert, J. Elucidating operating modes of bulk-heterojunction solar cells from impedance spectroscopy analysis. *J. Phys. Chem. Lett.* **2013**, *4*, 877–886. [CrossRef] [PubMed]
62. Guerrero, A.; Ripolles-Sanchis, T.; Boix, P.P.; Garcia-Belmonte, G. Series resistance in organic bulk-heterojunction solar devices: Modulating carrier transport with fullerene electron traps. *Org. Electron.* **2012**, *13*, 2326–2332. [CrossRef]
63. Yao, E.-P.; Chen, C.-C.; Gao, J.; Liu, Y.; Chen, Q.; Cai, M.; Hsu, W.-C.; Hong, Z.; Li, G.; Yang, Y. The study of solvent additive effects in efficient polymer photovoltaics via impedance spectroscopy. *Sol. Energy Mater. Sol. Cells* **2014**, *130*, 20–26. [CrossRef]
64. Basham, J.I.; Jackson, T.N.; Gundlach, D.J. Predicting the J-V curve in organic photovoltaics using impedance spectroscopy. *Adv. Energy Mater.* **2014**, *4*, 1400499. [CrossRef]
65. Guerrero, A.; Montcada, N.F.; Ajuria, J.; Etxebarria, I.; Pacios, R.; Garcia-Belmonte, G.; Palomares, E. Charge carrier transport and contact selectivity limit the operation of PTB7-based organic solar cells of varying active layer thickness. *J. Mater. Chem. A* **2013**, *1*, 12345–12354. [CrossRef]
66. Bhattacharya, S.; Dinda, D.; Saha, S.K. Role of trap states on storage capacity in a graphene/MoO_3 2D electrode material. *J. Phys. D Appl. Phys.* **2015**, *48*, 145303. [CrossRef]
67. Kalita, G.; Wakita, K.; Umeno, M.; Hayashi, Y.; Tanemura, M. Large-Area CVD. Graphene as transparent electrode for efficient organic solar cells. In Proceedings of the 2012 38th IEEE Photovoltaic Specialists Conference, Austin, TX, USA, 3–8 June 2012; pp. 3137–3141.
68. Choi, Y.-Y.; Kang, S.J.; Kim, H.-K.; Choi, W.M.; Na, S.-I. Multilayer graphene films as transparent electrodes for organic photovoltaic devices. *Sol. Energy Mater. Sol. Cells* **2012**, *96*, 281–285. [CrossRef]
69. Cha, M.J.; Kim, S.M.; Kang, S.J.; Seo, J.H.; Walker, B. Improved performance in flexible organic solar cells via optimization of highly transparent silver grid/graphene electrodes. *RSC Adv.* **2015**, *5*, 65646–65650. [CrossRef]
70. Lee, S.; Yeo, J.-S.; Ji, Y.; Cho, C.; Kim, D.-Y.; Na, S.-I.; Lee, B.H.; Lee, T. Flexible organic solar cells composed of P3HT: PCBM using chemically doped graphene electrodes. *Nanotechnology* **2012**, *23*, 344013. [CrossRef]